Localization and delocalization in networks with varied connectivity

Tamoghna Ray,[1,*] Amit Dey,[2,1,†] and Manas Kulkarni[1,‡]
[1]*International Centre for Theoretical Sciences, Tata Institute of Fundamental Research, Bengaluru 560089, India*
[2]*Ramananda College, Bankura University, Bankura 722122, India*

(Received 6 April 2022; accepted 26 September 2022; published 17 October 2022)

We study the phenomenon of localization and delocalization in a circuit-QED network with connectivity varying from finite-range coupling to all-to-all coupling. We find a fascinating interplay between interactions and connectivity. In particular, we consider (i) harmonic, (ii) Jaynes-Cummings, and (iii) Bose-Hubbard networks. We start with the initial condition where one of the nodes in the network is populated and then let it evolve in time. The time dynamics and steady state characterize the features of localization (self-trapping) in these large-scale networks. For the case of harmonic networks, exact analytical results are obtained, and we demonstrate that all-to-all connection shows self-trapping whereas the finite-ranged connectivity shows delocalization. The interacting cases (Jaynes-Cummings and Bose-Hubbard networks) are investigated both via exact quantum dynamics and via a semiclassical approach. We obtain an interesting phase diagram when one varies the range of connectivity and the strength of the interaction. We investigate the consequence of imperfections in the cavity or qubit and the role of inevitable disorder. Our results are relevant especially given recent experimental progress in engineering systems with long-range connectivity.

DOI: 10.1103/PhysRevA.106.042610

I. INTRODUCTION

The phenomenon of macroscopic self-trapping has been a subject of great interest and has been shown to occur in a variety of systems, both theoretically and experimentally. Notable examples include bosonic Josephson junctions (BJJs) consisting of cold-atomic Bose-Einstein condensates (BECs) [1–7] and photonic systems [8–13] characterized by light-matter interactions. Dissipative effects were also considered and the delocalization-localization transition of photons was theoretically predicted [12] in dissipative quantum systems and subsequently experimentally observed [13].

Although self-trapping was achieved, the inevitable photon leakage and spontaneous decay of the qubit limit the longevity of self-trapped states in realistic systems. To circumvent this, a drive was recently introduced, and it was shown theoretically that a delicate interplay between drive, dissipation, interaction, and kinetic hopping can lead to indefinitely-long-lived self-trapped states [14]. This was an important step forward as it provides a protocol to ensure indefinitely-long-lived localization in spite of cavity or qubit imperfections.

While most of the works above were either restricted to dimer systems or one-dimensional (1D) arrays, there is an important gap that needs to be addressed for the case when one has a highly nontrivial network of interacting systems. The properties of the network (such as connectivity) are expected to have an interesting impact on the phenomenon of localization and delocalization. This line of investigation is particularly important given recent experimental advances [15–23] in designing networks with varied connectivity (from finite range to long range) and success in establishing coupling between distant qubits [24–26]. The recent experimental designs are also amenable to an enhanced magnitude of connectivity. Additionally, such designs are tunable [27], scalable [26,28–30], generalizable to a wider range of platforms, and potentially relevant for quantum computation [15,16,19–23,31–33], modeling artificial light harvesters in fully connected networks [34,35], and quantum simulation schemes [17,23].

In this paper, we consider the circuit-QED network with varied connectivity which is shown schematically in Fig. 1. We consider a general setup where each unit is connected to other units (nodes) via a hopping term J that is preferably uniform between units. The connectivity may extend to a finite number of neighbors (Fig. 1, panel at right) or to all of them (Fig. 1, panel at left).

Each unit could in principle be any local Hamiltonian H_i, and we consider (i) harmonic, (ii) Jaynes-Cummings (JC), and (iii) Bose-Hubbard (BH) models. Our main results can be summarized as follows: (i) For harmonic networks, we present exact analytical results and highlight the clear distinction between finite-range and all-to-all coupling scenarios in terms of degree of photon localization. Here, one would naively expect that an excited unit of a harmonic network is prone to lose its excitation as its connectivity with the rest of the units increases. Surprisingly, this expected feature is contradicted by our observations. (ii) For the JC and BH networks, using both exact quantum and semiclassical approaches, we show the intricate interplay between connectivity and interactions, demonstrating self-trapped and delocalized regimes. (iii) Interesting nonmonotonic features in the degree of localization

*tamoghna.ray@icts.res.in
†amit.dey.85@gmail.com
‡manas.kulkarni@icts.res.in

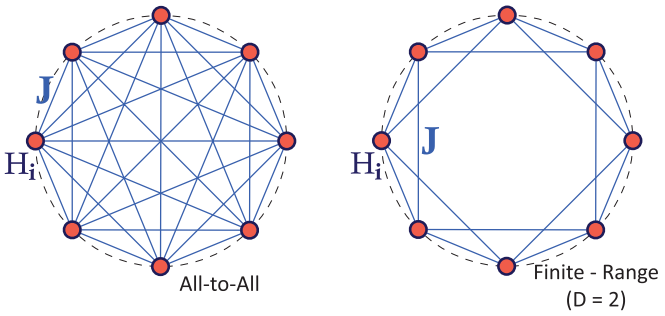

FIG. 1. A schematic representation of the circuit-QED network considered in this paper. The solid red circles denote the N units H_i, where we label $i = 0, 1, \ldots, N-1$, and the blue lines denote the interunit coupling with coupling strength J. The figure on the left indicates a network with all-to-all coupling, and the figure on the right indicates finite-range coupling with $D = 2$ nearest neighbors. One can note from the figure on the right that if $D \geqslant \lceil N/2 \rceil$ (where $\lceil\ \rceil$ denotes the ceiling function), then the unit effectively couples to all other units, which makes it fall under the all-to-all case.

are observed as one changes the number of units. (iv) The role of cavity dissipation, qubit decay or dephasing, and inevitable disorder has been highlighted.

II. THE HAMILTONIAN

We consider a system of N units H_i as shown in Fig. 1 which are connected to one another with a hopping term J. The Hamiltonian for such a system when there is all-to-all coupling is given by

$$H^{\text{all-all}} = \sum_{i=0}^{N-1} H_i - \frac{J}{2} \sum_{\substack{i,j=0 \\ i \neq j}}^{N-1} (a_i^\dagger a_j + \text{H.c.}), \tag{1}$$

where H_i is the Hamiltonian for the ith unit. Although in Eq. (1) we have considered all-to-all coupling, later on we will also present results for finite-neighbor coupling. In this study, we explore three different cases: harmonic, JC, and BH networks. In all these cases, bearing physical systems in mind, our objective is to study networks with varied sizes and connectivity keeping the hopping strength and total number of excitations fixed.

III. HARMONIC NETWORK

In the case of a harmonic network, $H_i = \omega_c a_i^\dagger a_i$, where ω_c is the cavity frequency and $a_i^\dagger$ and a_i are the creation and annihilation operators for the photons in the ith cavity. Such a system is exactly solvable, and we obtain analytical results for this network. We prepare the system in an initial state such that there are N_p bosons in the test unit ($i = 0$) and all other units are empty. The system is allowed to evolve in time, and one can compute observables such as the bosonic occupation at the ith unit, $n_i(t) = \langle a_i^\dagger(t) a_i(t) \rangle$, where $\langle\ \rangle$ is the quantum mechanical average. To study the dynamics of the bosons, we define the quantity $P(t) = n_0(t) - \sum_{j=1}^{N-1} n_j(t)$, which gives the population difference between the test unit and the rest of the system (imbalance). We introduce a convenient diagnostic tool to compute the degree of localization,

$$\eta = \frac{N_\text{p} + P_\text{min}}{2N_\text{p}}, \tag{2}$$

where P_min is the minimum value that $P(t)$ takes during its entire time evolution. Complete localization is characterized by $\eta \to 1$, and complete delocalization (i.e., all the photons have left the test unit) is characterized by $\eta \to 0$. For other values ($0 < \eta < 1$), the quantity η indicates the degree to which bosons in the test unit stay trapped.

To obtain the evolution of $P(t)$, we calculate the Heisenberg equations of motion (EOMs) of the system operators. For all-to-all coupling, we have (setting $\hbar = 1$)

$$\dot{a}_i = -i\omega_c a_i + iJ \sum_{\substack{j=0 \\ (j \neq i)}}^{N-1} a_j, \tag{3}$$

and for D-finite-neighbor coupling (note that $D < \lceil N/2 \rceil$), we have

$$\dot{a}_i = -i\omega_c a_i + iJ \sum_{d=1}^{D} (a_{i+d} + a_{i-d}). \tag{4}$$

When $D \geqslant \lceil N/2 \rceil$, we have the same setup as for all-to-all coupling. Equations (3) and (4) can be written as $\dot{\mathbf{x}} = \mathbf{A}\mathbf{x}$, where $\mathbf{x} = [a_0\ a_1 \cdots a_{N-1}]^T$. This can be solved by evaluating the eigenvalues $\{\lambda_\alpha\}$ and eigenvectors $\{\mathbf{u}_\alpha\}$ of $\mathbf{A}$ ($\alpha = 1, 2, \ldots, N$), i.e., $\mathbf{x}(\mathbf{t}) = \sum_{\alpha=1}^{N} c_\alpha e^{\lambda_\alpha t} \mathbf{u}_\alpha$, where c_α are the weights of the initial condition on the eigenvectors. We formulate an analytical solution for $P(t)$ by shifting to the Fourier space, $a_j^\dagger = \frac{1}{\sqrt{N}} \sum_{k=0}^{N-1} e^{-i\frac{2\pi}{N}kj} a_k^\dagger$. In this space, the Hamiltonian is diagonal,

$$H^{\text{finite}} = \omega_c \sum_{k=0}^{N-1} a_k^\dagger a_k - 2JDa_0^\dagger a_0 - 2J \sum_{k=1}^{N-1} f(k) a_k^\dagger a_k, \tag{5}$$

and $P(t)$ for D finite neighbors becomes (see Appendix A)

$$P(t) = \frac{2N_\text{p}}{N^2} \Bigg\{ 1 + \sum_{k,k'=1}^{N-1} \exp\left[i2Jt(f(k') - f(k))\right] + 2 \sum_{k=1}^{N-1} \cos\left[2Jt(f(k) - D)\right] \Bigg\} - N_\text{p}, \tag{6}$$

where

$$f(k) = \frac{\cos\left(\frac{D+1}{N}\pi k\right) \sin\left(\frac{D\pi k}{N}\right)}{\sin\left(\frac{\pi k}{N}\right)}. \tag{7}$$

For all-to-all coupling, we get

$$H^{\text{all-all}} = \omega_c \sum_{k=0}^{N-1} a_k^\dagger a_k - JNa_0^\dagger a_0 + JN_\text{p}, \tag{8}$$

and the imbalance becomes

$$P(t) = \frac{N_\text{p}}{N^2}[1 + (N-1)(N + 4\cos(NJt) - 3)]. \tag{9}$$

From Eqs. (9) and (2), we get

$$\eta = 1 - \frac{4}{N} + \frac{4}{N^2} \quad \text{(all-to-all coupling)}, \tag{10}$$

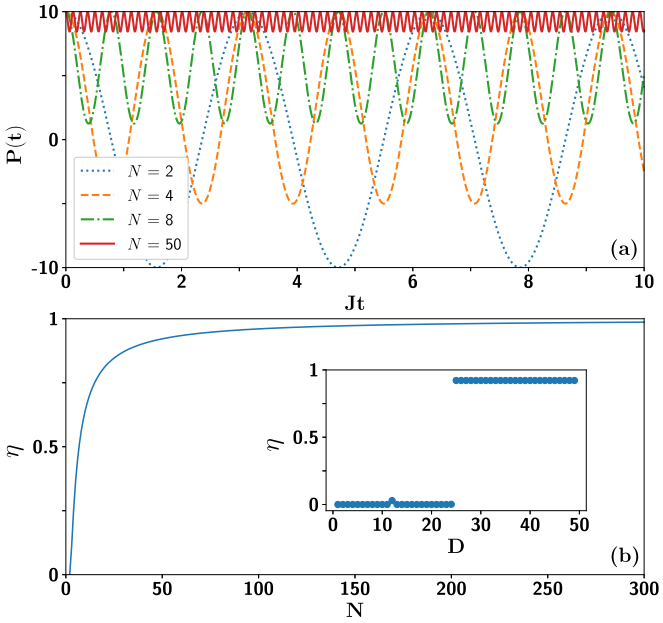

FIG. 2. (a) $P(t)$ obtained in Eq. (9) as a function of time (in units of $1/J$) for a harmonic network for varying number of units with all-to-all coupling. We prepare the system initially such that there are $N_p = 10$ bosons in the test unit. (b) η obtained in Eq. (10) as a function of N, clearly indicating stronger localization for large system sizes. The inset shows η as a function of the number of nearest neighbors D for $N = 50$, illustrating the loss of localization on losing the all-to-all configuration, i.e., when $D < \lceil N/2 \rceil$.

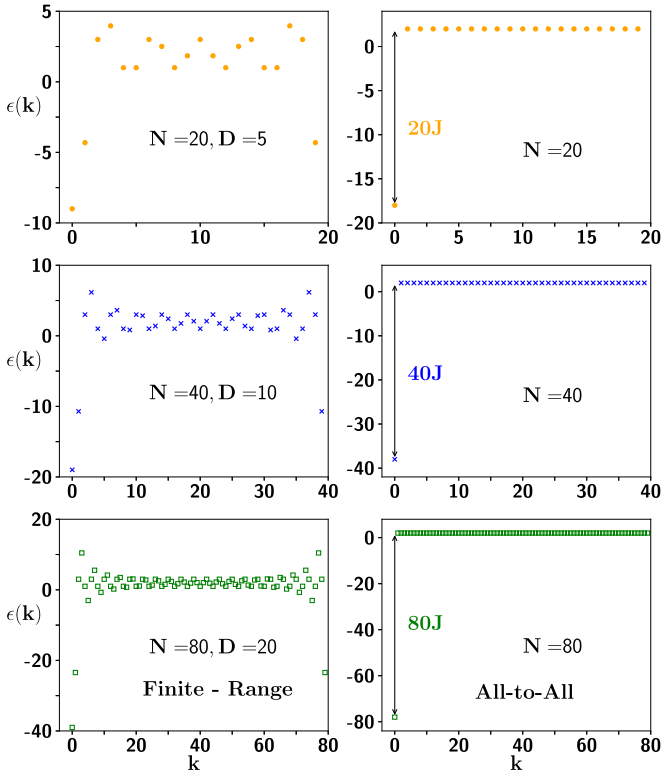

FIG. 3. Dispersion relation for the harmonic network with finite-range coupling for $N = 20$, 40, and 80 units with $D = 5$, 10, and 20 nearest neighbors, respectively (left panels), and all-to-all coupling for $N = 20$, 40, and 80 units (right panels). $\omega_c = 1$, and the energy is measured in units of J.

which implies that we achieve stronger localization of photons in the test unit as we increase the system size N. Note that $\lim_{N\to\infty} \eta = 1$ (for the all-to-all coupling case). In Fig. 2(a) we plot $P(t)$ as a function of time (in units of $1/J$) for all-to-all coupling. We notice that when the number of units is small there is delocalization (accompanied by oscillations). However, upon increasing the number of units the network tends to get more localized, and eventually there is perfect self-trapping in the large-N limit. Figure 2(b) shows the degree of localization η as one increases the number of units, which is given by Eq. (10). The inset in Fig. 2(b) demonstrates the loss of self-trapping in the finite-range case.

This phenomenon can be further understood by inspecting the dispersion relations in both the finite-range [Eq. (11)] and all-to-all [Eq. (12)] cases,

$$\epsilon^{\text{finite}}(k) = \omega_c - 2DJ\delta_{k,0} - 2Jf(k)(1-\delta_{k,0}), \tag{11}$$

$$\epsilon^{\text{all-all}}(k) = \omega_c - J(N-1)\delta_{k,0} + J(1-\delta_{k,0}). \tag{12}$$

A detailed derivation for the dispersion relations is provided in Appendix A.

The form of the dispersion relation in Eq. (12) reflects two important features of the system. Firstly, the eigenenergy spectrum $\epsilon(k)$ is nearly dispersionless (barring the $k = 0$ mode) as all the $k \neq 0$ modes have the same eigenenergy $\epsilon(k) = \omega_c + J$. Secondly, with increasing N the energy gap $|\epsilon(0) - \epsilon(k)| \sim N$ becomes wider, and the $k = 0$ mode is singled out from the large number of degenerate finite k modes (see Fig. 3, right panels). The imbalance $P(t)$ in the momentum space can be written as (see Appendix A)

$$P(t) = \frac{2}{N}\left\{\langle a_0^\dagger(t)a_0(t)\rangle + \sum_{k=1}^{N-1}\langle a_k^\dagger(t)a_0(t)\rangle + \sum_{k=1}^{N-1}\langle a_0^\dagger(t)a_k(t)\rangle + \sum_{k,k'=1}^{N-1}\langle a_k^\dagger(t)a_{k'}(t)\rangle\right\} - N_p. \tag{13}$$

From Eq. (8) it is clear that the evolution is determined only by $k = 0$ mode dynamics as $\sum_{k=0}^{N-1} a_k^\dagger a_k = N_p$. This implies that the time dependence of $P(t)$ is dictated by the second and third terms of Eq. (13). Terms $a_k^\dagger(t)a_0(t)$ amount to destroying one $k = 0$ mode boson and creating one with $k \neq 0$. This process becomes less probable or further suppressed as $|\epsilon(0) - \epsilon(k)|$ is enhanced (with increasing N). Therefore, for the large-N limit, the population in an all-to-all network does not evolve, and the bosons are completely stuck in the initial site. Here, we would like to make an important connection with the flat-band physics of localization. Flat bands, constituted by the dispersionless energy spectrum, retain the localization of the wave function in real space if the wave function is initially localized. Such a phenomenon has been experimentally observed in various contexts such as light localization in linear photonic lattices [36] and Mott-like electronic phases in graphene superlattices [37]. Engineered flat-band localization is an attractive topic in many-body physics [38], and such phases are accessible through bandwidth tuning [37,38]. In

our model, a flat band is closely achieved for the all-to-all case in the large-N limit. In contrast to this, for the finite-neighbor case [in Eq. (11)] neither are the $k \neq 0$ modes degenerate nor is there an enhanced gap between $k = 0$ and $k \neq 0$ modes even for large N (see Fig. 3, left panels). This leads to the dynamics of $P(t)$ [see Eq. (6)] and subsequent photon delocalization.

It is worth noting that alternatively, we can numerically compute the entire correlation $N \times N$ matrix $C(t) = \langle \mathbf{x}(t)\mathbf{x}^{\dagger}(t)\rangle$ which is given by $C(t) = e^{-iht}C(0)e^{iht}$, where h is the single-particle Hamiltonian (the $N \times N$ matrix which contains information as to whether the network connectivity is finite range or all to all) that appears in $H = \sum_{i,j=0}^{N-1} h_{ij}a_i^{\dagger}a_j$. From $C(t)$, we can extract $P(t) = 2C_{00}(t) - \mathrm{tr[C(t)]} + (\mathrm{N} - 2)$, and this is in perfect agreement with our analytical expressions derived above [Eqs. (6) and (9)]. Next, we discuss the case of on-site interactions or anharmonicity.

IV. JAYNES-CUMMINGS NETWORK

One can envision a situation where each cavity hosts a qubit. This leads to the well-known Jaynes-Cummings system, whose Hamiltonian is given by

$$H_i = \omega_c a_i^{\dagger}a_i + \omega_q \sigma_i^{+}\sigma_i^{-} + g(a_i\sigma_i^{+} + a_i^{\dagger}\sigma_i^{-}), \tag{14}$$

where ω_c and ω_q are the cavity frequency and the energy gap of the qubit, respectively, g is the cavity-qubit coupling strength, and σ_i^{+} and σ_i^{-} are the raising and lowering operators for the ith qubit, respectively. For the case of $N = 2$ (a dimer), the delocalization-localization transition was investigated theoretically [12] and was subsequently observed experimentally [13]. Recently, the intricate role of drive in circumventing inevitable imperfections was investigated for the JC dimer and a 1D array leading to the proposal of an indefinitely-long-lived self-trapped state [14]. Given recent experimental advances in designing highly connected networks (which is a nontrivial generalization of a dimer), we consider the setup with fully long-range (all-to-all) and finite-range connectivities. Each unit H_i is described by Eq. (14), and these units sit in networks such as the ones shown in Fig. 1. The role of light-matter interaction g and the number of neighbors D in the dynamics in such networks is investigated for the resonant case ($\omega_c = \omega_q$). The system therefore is an ideal platform for understanding the intricate interplay between network connectivity D, interactions g, and kinetic hopping J.

We present an exact quantum solution for Eq. (3) where H now stands for the JC network. The system is initially prepared with all the excitations (N_p) in the cavity mode of the test unit, and all other cavities and qubits are kept in the ground state, i.e., $n_0(0) = N_\mathrm{p}$, $n_{i\neq 0}(0) = 0$, and $\langle \sigma_i^z(0)\rangle = -1$. Since there is no drive in the system, the oscillators can never be excited beyond $|N_\mathrm{p}\rangle$ (in each unit), and hence we truncate the basis at $|N_\mathrm{p}\rangle$. The dimension $\mathcal{N}_d$ of this truncated Hilbert space for the entire system is given by $\mathcal{N}_d = [2(N_p + 1)]^N$. For five units and ten photons, $\mathcal{N}_d = 22^5$ (larger than 2^{22}), and we numerically evolve the system with the Hamiltonian for these parameters. In Fig. 4, we investigate $P(t)$ as a function of time. One can notice that for small g the photons delocalize and, for large g, the photons are localized in the test unit.

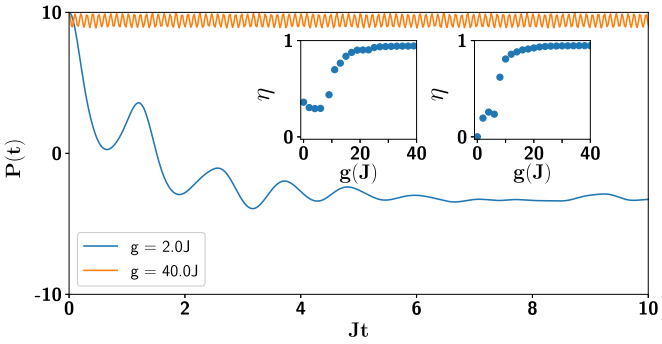

FIG. 4. The population imbalance $P(t) = n_0(t) - \sum_{j=1}^{N-1} n_j(t)$ as a function of t (in units of $1/J$) is plotted for a network of $N = 5$ JC units (resonant case $\omega_c = \omega_q$) for different values of g using exact quantum numerics. This is the case of all-to-all coupling where the initial condition is such that there are $N_\mathrm{p} = 10$ photons in the test unit and the rest of the units are empty. Qubits in all units are initially assumed to be in the ground state. It is evident from the figure that for weak interactions g, one gets delocalization, and we reach a self-trapped state when we increase the interaction. The left and right insets show the degree of localization as a function of g (in units of J) for the all-to-all coupling and nearest-neighbor coupling cases, respectively.

This self-trapped phenomenon for large g is a result of an interesting interplay between interaction, kinetic hopping, and network connectivity. Figure 4 has two insets. The left inset shows the degree of localization as one tunes the interaction strength g for the all-to-all coupling case, and the right inset demonstrates it for the nearest-neighbor (NN) coupling case, clearly highlighting the consequence of all-to-all connectivity. Even for small values of g the first case (all to all) shows partial localization, whereas we see complete delocalization in the second case (nearest neighbor).

Since the dimension $\mathcal{N}_d$ of the Hilbert space is very large, it is evident that simulating this system with exact quantum numerics for larger N is essentially impossible. Therefore, to analyze the behavior of large networks, we resort to a semiclassical approximation where we decouple correlation functions, such as $\langle a_i\sigma_i^z\rangle \approx \langle a_i\rangle\langle\sigma_i^z\rangle$. When feasible, we have benchmarked semiclassical results with direct quantum simulations thereby supporting the usage of the semiclassical approach (see Appendix B). Introducing the definitions $\langle a_i\rangle \equiv \alpha_i$, $\langle\sigma_i^-\rangle \equiv \beta_i$, and $\langle\sigma_i^z\rangle \equiv w_i$, the semiclassical EOMs for all-to-all connectivity are given by

$$\dot{\alpha}_i = -i\omega_c\alpha_i + iJ\sum_{\substack{j=0\\(j\neq i)}}^{N-1}\alpha_j - ig\beta_i, \tag{15}$$

$$\dot{\beta}_i = -i\omega_q\beta_i + ig\alpha_i w_i, \quad \dot{w}_i = 2ig(\alpha_i^*\beta_i - \alpha_i\beta_i^*). \tag{16}$$

Such an approximation typically fails for small photon numbers, where quantum fluctuations play a significant role. In Fig. 5(a), we show the heat map for the degree of localization as one varies the light-matter interaction strength g and the range of connectivity of the network D. We see that for a given range of connectivity there exists a critical value of g which demarcates the delocalization-localization transition. In agreement with the left inset in Fig. 4, we observe that

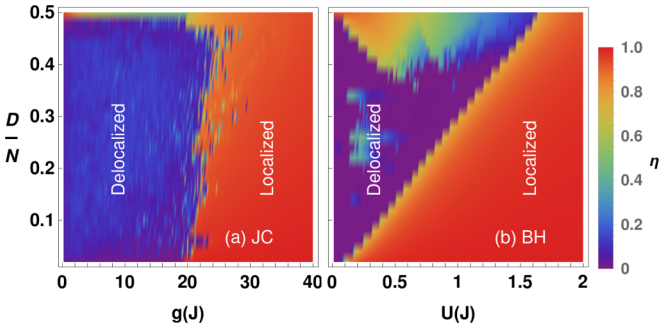

FIG. 5. Heat map for η with varying the numbers of nearest neighbors D (as a fraction of the total number of units) and interactions for (a) JC and (b) BH using the semiclassical approach. The parameters are $N = 50$ and $N_p = 50$. For the JC network the resonant case, i.e., $\omega_c = \omega_q$, is considered. We find a transition from the delocalized to the self-trapped regime.

for the case of all-to-all connectivity ($D/N = 0.5$), the system is in the localized phase irrespective of the interaction strength g, whereas for the case of NN coupling we observe complete delocalization for smaller values of g as indicated in the right inset in Fig. 4. However, the value of η might vary depending on the system size as indicated in Sec. III. The results presented here are for the resonant case ($\omega_c = \omega_q$) and therefore correspond to the case of strongly anharmonic cavity networks. Our results are generalizable to the off-resonant JC case ($\omega_c \neq \omega_q$). A well-known limit is the dispersive JC case, where the detuning between the cavity and qubit frequencies is large compared with light-matter interactions g. In this limit, the system can map to an attractive or repulsive BH network [39]. Irrespective of this connection between a dispersive JC network and a BH network, the BH network with varied connectivity is a fascinating many-body system in itself and warrants a thorough investigation, which is done next.

V. NETWORK WITH BOSE-HUBBARD NONLINEARITY

The governing Hamiltonian for the Bose-Hubbard system is the same as in Eq. (1) with the ith unit described by the Hamiltonian $H_i = \omega_c a_i^\dagger a_i - \frac{U}{2} n_i^2$. Here, U quantifies the strength of on-site attractive interaction. Our analysis involves networks with a large number of cavity units and large photon numbers. Tackling such a large-scale system is beyond the scope of a fully quantum treatment due to numerical complexity. Considering the success of semiclassical theory in analyzing BH systems [1,3,5,40–42], we employ the semiclassical approximation for our system and write the EOM for all-to-all connectivity as

$$\dot{\alpha}_i = -i\omega_c \alpha_i + iJ \sum_{\substack{j=0 \\ (j\neq i)}}^{N-1} \alpha_j + iU|\alpha_i|^2 \alpha_i, \tag{17}$$

where $\langle a_i \rangle \equiv \alpha_i$. We initiate the system by populating just the test unit, i.e., $\alpha_0 = \sqrt{10}$ with the rest of them taken to be empty, i.e., $\alpha_{j\neq 0} = 0$.

With these initial conditions, we numerically solve the set of coupled nonlinear differential equations [Eq. (17)] and plot $P(t)$ in Fig. 6(a). We observe that the localization deteriorates as the number of units N increases from 2 to 8. This feature is exactly opposite to the linear cavity network discussed earlier. Interestingly, with a further increase of N from 8 to 50, Fig. 6(a) shows enhancement of localization. In other words, beyond a certain N (say, N^*) the system behaves similarly to an almost linear network (the effect of U is of course still there). This nonmonotonic feature is clearly visible in Fig. 6(b) for three different values of U. The vertical dashed lines mark the N^* where the system transits from nonlinear to almost linear in terms of localization. It is also important to note that the transition point N^* moves towards higher values as U is increased, and the detailed relationship between N^* and U is captured in the inset of Fig. 6(b). We further investigate the role of connectivity in Fig. 6(c), where we plot the degree of localization η as a function of D for $N = 50$ units and $N_p = 20$ photons. For lower values of U ($= J,\ 2J$), we observe that η initially decreases to 0 and then again increases to its all-to-all connectivity value after being completely delocalized over a range of D. For higher values

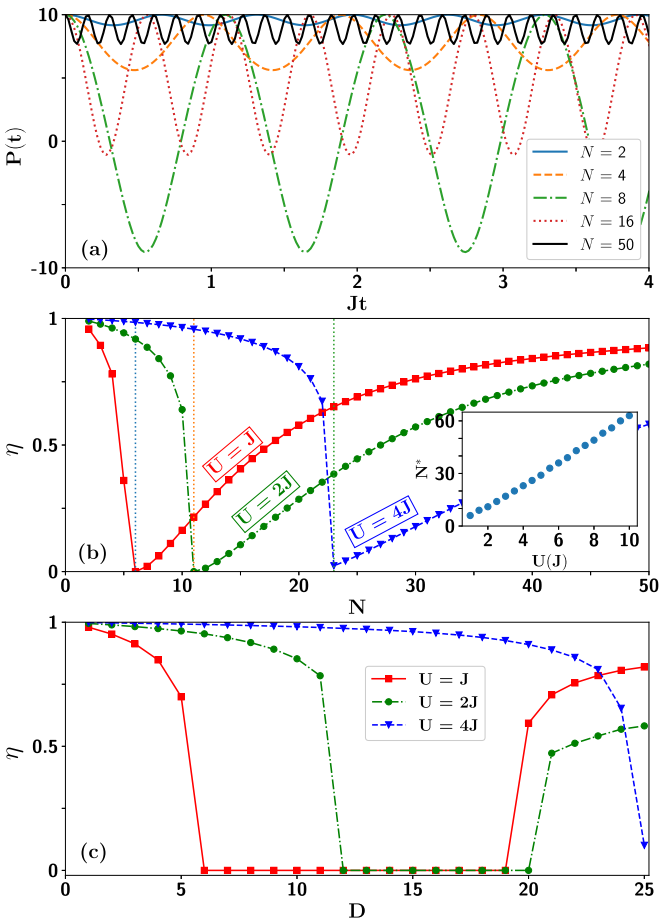

FIG. 6. (a) $P(t)$ as a function of time (in units of $1/J$) when uniform on-site nonlinearity (all-to-all BH network) is present in each cavity with $U = J$ for various values of N. (b) Degree of localization vs N for various values of BH nonlinearity for the all-to-all network. The dashed vertical lines mark the threshold number N^* after which the network resembles a linear behavior. The inset shows the behavior of N^* as a function of BH nonlinearity U. (c) Degree of localization as a function of the number of neighbors D for various values of U ($N = 50$, $N_p = 20$).

of U ($= 4J$), the system is never in the completely delocalized state; rather it falls from complete localization to its all-to-all connectivity value. The initial fall in η takes place due to the increase in the number of pathways for the photons to escape; however, for higher values of D, the system closely resembles the all-to-all configuration, and thus η increases again. For higher U, the effect of connectivity is dominated over by the on-site attractive interaction. In Fig. 5(b) we investigate the role of D and U in η for $N = 50$ and $N_p = 50$. A clear transition from the delocalized to the self-trapped regime is observed, and there is a linear relationship between the value of U at which the transition takes place and the number of neighbors. In the delocalized phase we observe a regime of localized phase on increasing D/N. The phase boundary here is a nontrivial function of U and D/N. Another region or patch of slightly increased η is visible around $U = 0.2J$ and $D/N \in (0.20, 0.35)$ which is an artifact of semiclassical approximation.

The nonlinear cavity in the all-to-all network contains rich physics of competing factors such as U and N. On the one hand, increasing the number of units N increases the number of pathways for the movement of photons. On the other hand, the BH interaction U restricts photon flow due to on-site photon-photon attraction. This is the reason that the degree of localization decreases when one increases N for a fixed U. However, after crossing some threshold N^* the degree of localization improves because the system closely resembles a linear system. Needless to mention, it is paramount to establish that this nonmonotonic behavior is not an artifact of semiclassical approximation [Eq. (17)]. To do so, when feasible we perform an exact quantum calculation and demonstrate the nonmonotonic feature (see Appendix B).

VI. CONCLUSIONS AND OUTLOOK

Macroscopic self-trapping (or lack thereof) is a phenomenon that has been a subject of intense investigation in various physical platforms. We fill a major gap in this direction by studying localization physics in scalable circuit-QED networks with connectivity that can be varied from finite range to fully long range. For the case of harmonic networks we demonstrate localization that is rooted in all-to-all connectivity as opposed to disorder [43] or interactions [5,44]. Here it is worth mentioning that the disorder-induced localization phenomenon has been studied in lattices with different topologies [45–48]. Furthermore, localization physics and its dependence on coordination number have been analyzed on random regular graphs, which are important tools for solving many-body problems [47,48]. After providing analytical results for the harmonic network, we unveiled the exotic interplay between anharmonicity or interactions, kinetic hopping, and network connectivity that often leads to counterintuitive behavior. We observe that as we increase the strength of interaction, the effect of connectivity is suppressed, and the localization phenomenon is dictated primarily by interactions. Such interplay is expected to be robust to different types of local interactions. In fact, to highlight this universality, we used two entirely different types of local interactions, namely, (i) Jaynes-Cummings and (ii) Bose-Hubbard interactions. In this context it is important to mention that many-body localization has been extensively studied in networks where interactions and disorder play pivotal roles [49–52]. We present exact quantum numerics for feasible system sizes and study large-scale networks using a semiclassical approach. When possible, we perform a comparative study between quantum and semiclassical approaches (Appendix B). Bearing in mind realistic experimental setups, we investigate the role of imperfections in the cavity or qubit and disorder. Our open quantum system computations (Appendix C) show that for experimentally accessible time scales one can still capture the interesting results of localization. We also demonstrate robustness to disorder (Appendix D).

Our findings are relevant for physical systems with long-range connectivity. In recent experiments related to large quantum computational architectures, designing nontrivial geometry and engineering connectivity through multiple qubits have become objects of increasing focus [16–18,53,54]. Our findings are potentially experimentally realizable in existing circuit-QED platforms and are expected to play a pivotal role in exploring other setups with nontrivial geometries. Our investigation reveals experimentally realizable regimes where the system retains information about its initial state and hence provides a possible platform to store quantum information [55,56]. As a future direction, it would be interesting to consider driven-dissipative quantum networks (with varied connectivity) and investigate their nonequilibrium steady-state properties. It is worth noting that the network configuration also contains rich chaotic regimes. The impact of chaos on population or state transfer in large networks is another interesting future aspect of study [57]. It is challenging and interesting to explore level spacing statistics (and spectral transitions) in these networks, and this is expected to have a deep connection to the localization or delocalization phenomena [58]. Our work can be further extended to more interesting geometries such as hyperbolic lattices [59,60]. Such exotic deformations of lattices have been realized in experiments using coplanar waveguide resonators [59], and it would be interesting to investigate the effect of curvature along with connectivity on such networks.

ACKNOWLEDGMENTS

We thank R. Vijayaraghavan, S. Hazra, D. O'Dell, H. K. Yadalam, S. Roy, A. Vardi, and S. Yarlagadda for useful discussions. M.K. acknowledges the support of the Ramanujan Fellowship (SB/S2/RJN-114/2016), SERB Early Career Research Award (ECR/2018/002085), and SERB Matrics Grant (MTR/2019/001101) from the Science and Engineering Research Board (SERB), Department of Science and Technology, Government of India. M.K. acknowledges the support of the Department of Atomic Energy, Government of India, under Project No. RTI4001. We gratefully acknowledge the ICTS-TIFR for use of its high-performance computing facility. M.K. thanks the École Normale Supérieure (Paris) for hospitality.

APPENDIX A: ANALYTICAL RESULTS FOR HARMONIC NETWORKS

In this Appendix, we will derive analytical expressions for $P(t)$ in both the finite-range coupling (Sec. A 1) and all-to-

all coupling (Sec. A 2) cases when the units H_i are harmonic oscillators, i.e., $H_i = \omega_c a_i^\dagger a_i$. We shift to the Fourier space,

$$a_j^\dagger = \frac{1}{\sqrt{N}} \sum_{k=0}^{N-1} e^{-i\frac{2\pi}{N}kj} a_k^\dagger, \tag{A1}$$

where $j = 0, 1, 2, \ldots, N-1$ is the lattice index and k represents the wave number. Substituting Eq. (A1) into the unit Hamiltonian we get

$$\sum_{j=0}^{N-1} H_j = \frac{\omega_c}{N} \sum_{\substack{k,k'=0 \\ j=0}}^{\substack{k,k'=N-1 \\ j=N-1}} a_k^\dagger a_{k'} e^{-i\frac{2\pi}{N}(k-k')j}. \tag{A2}$$

Now using the Fourier decomposition of the Kronecker delta,

$$\frac{1}{N} \sum_{j=0}^{N-1} e^{-i\frac{2\pi}{N}(k-k')j} = \delta_{kk'}, \tag{A3}$$

we get rid of the sum over j and contract the sum over k', which finally yields

$$\therefore \sum_{j=0}^{N-1} H_j = \omega_c \sum_{j=0}^{N-1} a_j^\dagger a_j = \omega_c \sum_{k=0}^{N-1} a_k^\dagger a_k. \tag{A4}$$

Now, to evaluate the coupling Hamiltonian, we will need to simplify terms such as $\sum_{j=0}^{N-1}(a_j^\dagger a_{j+d} + \text{H.c.})$, where d is some integer. Performing a Fourier transform gives

$$\sum_{j=0}^{N-1}(a_j^\dagger a_{j+d} + \text{H.c.}) = \frac{1}{N} \sum_{\substack{k,k'=0 \\ j=0}}^{\substack{k,k'=N-1 \\ j=N-1}} \left(e^{-i\frac{2\pi}{N}kj + i\frac{2\pi}{N}k'(j+d)} a_k^\dagger a_{k'} + \text{H.c.}\right). \tag{A5}$$

Again, using Eq. (A3) and contracting the sum over k', we get

$$\sum_{i=0}^{N-1}(a_i^\dagger a_{i+d} + \text{H.c.}) = 2\sum_{k=0}^{N-1} a_k^\dagger a_k \cos\left(\frac{2\pi}{N}kd\right). \tag{A6}$$

1. Finite-range coupling

For finite-range coupling ($D < \lceil N/2 \rceil$), using Eq. (A6), the coupling part of the Hamiltonian ($H_{\text{coupl.}}$) becomes

$$\begin{aligned} H_{\text{coupl.}}^{\text{finite}} &= -J \sum_{i=0}^{N-1} \sum_{d=1}^{D} (a_i^\dagger a_{i+d} + \text{H.c.}) \\ &= -2J \sum_{k=0}^{N-1} \sum_{d=1}^{D} \cos\left(\frac{2\pi}{N}kd\right) a_k^\dagger a_k \\ &= -2JDa_0^\dagger a_0 - 2J \sum_{k=1}^{N-1} f(k) a_k^\dagger a_k, \end{aligned} \tag{A7}$$

where

$$f(k) = \sum_{d=1}^{D} \cos\left(\frac{2\pi}{N}kd\right) = \frac{\cos\left(\frac{D+1}{N}\pi k\right)\sin\left(\frac{D\pi k}{N}\right)}{\sin\left(\frac{\pi k}{N}\right)}. \tag{A8}$$

From Eqs. (A4) and (A7) we can write down the dispersion relation for the finite range as

$$\epsilon^{\text{finite}}(k) = \omega_c - 2DJ\delta_{k,0} - 2Jf(k)(1 - \delta_{k,0}). \tag{A9}$$

Using $\dot{a_k} = i[H, a_k]$, where H is in the momentum basis, the equations of motion become

$$\dot{a_k} = \begin{cases} -i\omega_c a_k + i2Jf(k)a_k, & k \neq 0 \\ -i\omega_c a_k + i2JDa_k, & k = 0. \end{cases} \tag{A10}$$

Note that in the above equation (A10), we treat the $k \to 0$ limit carefully and separately. The solution to Eq. (A10) reads

$$a_k(t) = \begin{cases} a_k(0)\exp[-i(\omega_c - 2Jf(k))t], & k \neq 0 \\ a_k(0)\exp[-i(\omega_c - 2DJ)t], & k = 0. \end{cases} \tag{A11}$$

The initial values $a_k(0)$ are determined by $a_j(0)$ using Eq. (A1),

$$a_k(0) = \frac{1}{\sqrt{N}} \sum_{j=0}^{N-1} e^{-ikj} a_j(0). \tag{A12}$$

Now we initiate the system in such a way that there are N_{p} bosons in the test unit and all other sites are empty, i.e., $\langle a_0(0)\rangle = \sqrt{N_{\text{p}}}$ and $\langle a_{j\neq 0}(0)\rangle = 0$. Therefore we have

$$\langle a_k(0)\rangle = \sqrt{\frac{N_{\text{p}}}{N}}. \tag{A13}$$

The population difference operator $P(t)$ can be written as

$$P(t) = 2n_0(t) - \sum_{j=0}^{N-1} n_j(t), \tag{A14}$$

where we recall that $n_i(t) = \langle a_i^\dagger(t) a_i(t)\rangle$. Since there are no dissipative processes involved, we have $\sum_{j=0}^{N-1} n_j(t) = N_{\text{p}}$. Using Eq. (A1), we get

$$\begin{aligned} P(t) &= \frac{2}{N} \sum_{k,k'=0}^{N-1} \langle a_k^\dagger a_{k'}\rangle - N_{\text{p}} \\ &= \frac{2}{N}\left\{\langle a_0^\dagger(t)a_0(t)\rangle + \sum_{k=1}^{N-1}\langle a_k^\dagger(t)a_0(t)\rangle \right. \\ &\quad \left. + \sum_{k=1}^{N-1}\langle a_0^\dagger(t)a_k(t)\rangle + \sum_{k,k'=1}^{N-1}\langle a_k^\dagger(t)a_{k'}(t)\rangle\right\} - N_{\text{p}}. \end{aligned} \tag{A15}$$

Substituting Eqs. (A11) and (A13), we get

$$\begin{aligned} P(t) = \frac{2N_{\text{p}}}{N^2}\left\{1 + \sum_{k,k'=1}^{N-1} \exp\left[i2Jt(f(k') - f(k))\right]\right. \\ \left. + 2\sum_{k=1}^{N-1}\cos\left[2Jt(f(k) - D)\right]\right\} - N_{\text{p}}. \end{aligned} \tag{A16}$$

2. All-to-all coupling

For all-to-all coupling and for $D \geqslant \lceil N/2 \rceil$ we follow the same steps as in the case of finite-range coupling, with the

necessary changes in the coupling term.

$$
\begin{aligned}
H_{\text{coupl.}}^{\text{all-all}} &= -\frac{J}{2}\sum_{\substack{i,j=0\\ i\neq j}}^{N-1}(a_i^\dagger a_j + \text{H.c.}) \\
&= -J\sum_{k=0}^{N-1}\sum_{d=1}^{N-1}\cos\left(\frac{2\pi}{N}kd\right)a_k^\dagger a_k \\
&= -J(N-1)a_0^\dagger a_0 \\
&\quad - J\sum_{k=1}^{N-1}\frac{\cos(\pi k)\sin\left(\frac{N-1}{N}\pi k\right)}{\sin\left(\frac{\pi k}{N}\right)}a_k^\dagger a_k \\
&= -J(N-1)a_0^\dagger a_0 + J\sum_{k=1}^{N-1}a_k^\dagger a_k \\
&= -JNa_0^\dagger a_0 + JN_{\text{p}}. \qquad \text{(A17)}
\end{aligned}
$$

From Eqs. (A4) and (A17) we can write down the dispersion relation for the all-to-all coupling case as

$$\epsilon^{\text{all-all}}(k) = \omega_c - J(N-1)\delta_{k,0} + J(1-\delta_{k,0}). \qquad \text{(A18)}$$

Now, the equations of motion are given by

$$\dot{a}_k = \begin{cases} -i\omega_c a_k - iJa_k, & k \neq 0 \\ -i\omega_c a_k + iJ(N-1)a_k, & k = 0, \end{cases} \qquad \text{(A19)}$$

whose solution reads

$$a_k(t) = \begin{cases} a_k(0)e^{-i(\omega_c+J)t}, & k \neq 0 \\ a_k(0)e^{-i(\omega_c-(N-1)J)t}, & k = 0. \end{cases} \qquad \text{(A20)}$$

Substituting Eq. (A20) into Eq. (A15), we get

$$
\begin{aligned}
P(t) = \frac{2}{N}\Bigg\{&\frac{N_{\text{p}}}{N} + \frac{N_{\text{p}}}{N}(N-1)^2 \\
&+ \frac{N_{\text{p}}}{N}(N-1)2\cos(NJt)\Bigg\} - N_{\text{p}}. \qquad \text{(A21)}
\end{aligned}
$$

Rearranging the terms in Eq. (A21), we get

$$P(t) = \frac{N_{\text{p}}}{N^2}[1 + (N-1)(N + 4\cos(NJt) - 3)]. \qquad \text{(A22)}$$

APPENDIX B: COMPARISON BETWEEN EXACT QUANTUM COMPUTATIONS AND THE SEMICLASSICAL APPROACH

This Appendix is dedicated to comparing (whenever feasible) exact quantum computations with the semiclassical approach. This is of paramount importance since both the JC and BH networks are nonlinear systems and hence doing exact quantum calculations becomes unfeasible beyond a point. Therefore it is important to have a benchmark so that one can use the semiclassical approach for larger-scale problems. As mentioned in Sec. IV, the dimension $\mathcal{N}_d$ of the Hilbert space for the entire system of the JC network is extremely large and is given by $\mathcal{N}_d = [2(N_{\text{p}}+1)]^N$. For example, if the number of units is $N = 5$ and we take $N_{\text{p}} = 10$ photons, then $\mathcal{N}_d = 22^5$ (which is larger than 2^{22}). This means that beyond a few units, the exact quantum calculations become unfeasible and one needs to resort to other approaches such as the semiclassical method.

In Fig. 7, we demonstrate the agreement between exact quantum numerics and semiclassical results for the JC and BH networks for both finite-range and all-to-all coupling. In particular, we investigate the degree of localization as a function of the strength of the nonlinearity. We find that even the quantitative agreement is reasonably good.

As a consequence of this agreement between semiclassical and exact quantum methods, we elaborate on the nonmonotonic behavior of localization for the BH network that was shown in Fig. 6(b). A natural question is whether this nonmonotonic behavior (η versus N) is a consequence of semiclassical approximation or whether it is also present in fully quantum calculations. In Fig. 6(b), we have shown the nonmonotonic behavior of localization for BH nonlinearity by considering semiclassical theory. Here, we will show that this nonmonotonic behavior can also be verified for the quantum case. We observe in Fig. 6(b) that, in between the first two vertical dashed lines, localization for the $U = J$ case is better when N is larger (the solid red line is curving upwards). On the other hand, for $U = 2J$, the degree of localization decreases when N increases (the green dashed-dotted line is curving downwards). This is rooted in the fact that, upon increasing N, the $U = J$ case enters the linearlike region earlier than the $U = 2J$ case. This implies that for two values of N, say, $N = 3$ and $N = 4$, the saturation values of $P(t)$ would have the opposite trend for $U = J$ and $U = 2J$. We find this also

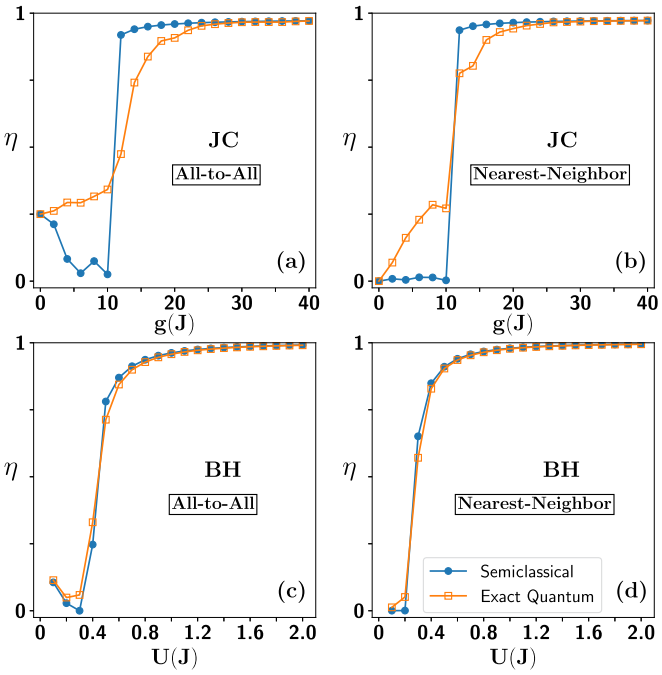

FIG. 7. Comparison of exact quantum numerics and semiclassical approach. (a) and (b) show η as a function of g (in units of J) for the JC network with $N = 4$ and $N_{\text{p}} = 20$, for all-to-all and nearest-neighbor coupling, respectively. (c) and (d) show η as a function of U (in units of J) for the BH network with $N = 4$ and $N_{\text{p}} = 20$, for all-to-all and nearest-neighbor coupling, respectively.

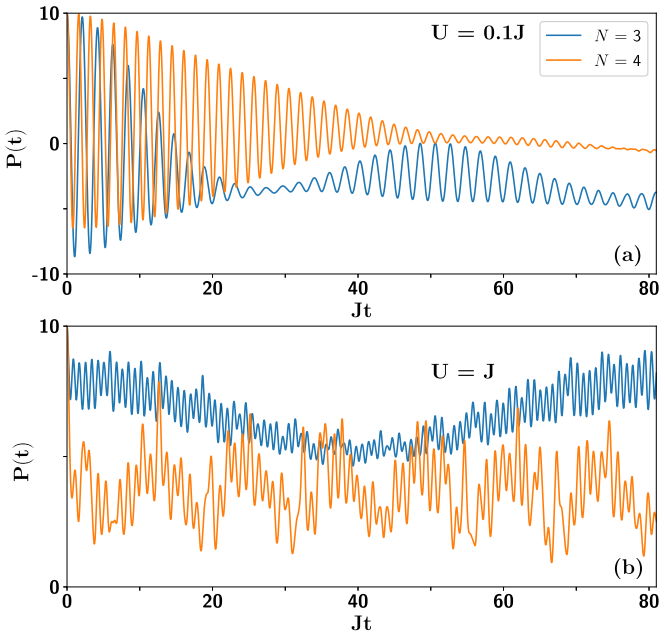

FIG. 8. Results of fully quantum treatment for the BH network ($N = 3, 4$ and $N_p = 10$) with all-to-all connectivity. The population difference is shown for (a) $U = 0.1J$ and (b) $U = J$ as a function of time (in units of $1/J$). It is clear that for $U = 0.1J$ the case of $N = 4$ is more localized whereas for $U = J$ the case of $N = 3$ is more localized thereby showing nonmonotonicity in the quantum case.

to be true when we perform the exact quantum calculations. Comparing Figs. 8(a) and 8(b), we see that the population difference $P(t)$ for the $N = 4$ case lies above the $N = 3$ case when $U = 0.1J$, whereas the order is reversed for the $U = J$ case. Therefore this feature is consistent with the observation we have for the semiclassical case and is a reflection of nonmonotonicity.

APPENDIX C: CLOSED VERSUS OPEN QUANTUM SYSTEMS

In this Appendix, we investigate the consequence of imperfections due to coupling with the environment, which are inevitable in physical systems. Examples of such imperfections include dissipation in the cavity and qubit decay or dephasing. In this paper, we neglected environmental effects to focus mainly on the interplay between nonlinearity, kinetic hopping, and connectivity. Here, we discuss the case in which we have open quantum systems. The ranges of parameters that we consider are motivated by experiments and summarized in Table I. To incorporate environmental effects in the system dynamics, we rely on the Lindblad formalism and exploit the following local Lindblad quantum master equation:

$$\dot{\rho}(t) = -i[H, \rho(t)] + \kappa \sum_{j=0}^{N-1} \mathcal{L}[a_j] + \gamma \sum_{j=0}^{N-1} \mathcal{L}[\sigma_j^-] + \gamma_\phi \sum_{j=0}^{N-1} \mathcal{L}[\sigma_j^z], \tag{C1}$$

TABLE I. Summary of the typical range of parameter values obtainable in circuit-QED [13,16,61–63].

	Typical range of parameter values ($\times 2\pi$)
ω_c	4–8 GHz
ω_q	4–8 GHz
g	1–300 MHz
U	150–350 MHz
J	50 kHz to 50 MHz
κ	50 kHz to 50 MHz
γ	20–200 kHz
γ_ϕ	20–200 kHz

where $\mathcal{L}[A_j] = (2A_j\rho(t)A_j^\dagger - A_j^\dagger A_j\rho(t) - \rho(t)A_j^\dagger A_j)/2$. $\rho(t)$ is the reduced density matrix of the system, which is obtained by tracing out the environmental degrees of freedom from the full density matrix (of the system and the environment). It is important to note that we restrict ourselves to local Lindblad description although, in general, a rigorous derivation starting from a microscopic system-bath Hamiltonian is expected to lead to various variants of quantum master equations [64] depending on the parameter regimes. Furthermore, we consider the very low temperature T regime and neglect the effect of thermal excitations in Eq. (C1). This is because typical temperature regimes in experiments range from $T \sim 10$ mK to $T \sim 30$ mK. For BH networks, qubit degrees of freedom are absent, and the governing Lindblad master equation can

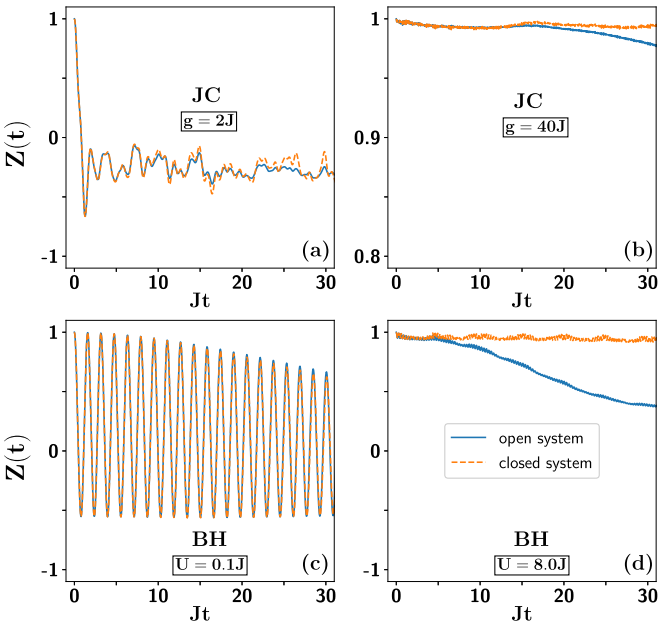

FIG. 9. Comparison of exact quantum numerics for closed and open systems. (a) and (b) show the evolution of $Z(t)$ defined in Eq. (C2) as a function of time (in units of $1/J$) for the JC network with $N = 3, N_p = 5, \kappa = 0.01J, \gamma = 0.01J$, for $g = 2J$ and $g = 40J$, respectively. (c) and (d) show the evolution of $Z(t)$ as a function of time (in units of $1/J$) for the BH network for $U = 0.1J$ and $U = 8J$, respectively ($N = 4$, $N_p = 4$, $\kappa = 0.01J$). In both cases, all-to-all coupling is considered. This figure clearly demonstrates the intricate interplay between connectivity, interaction, and dissipation channels.

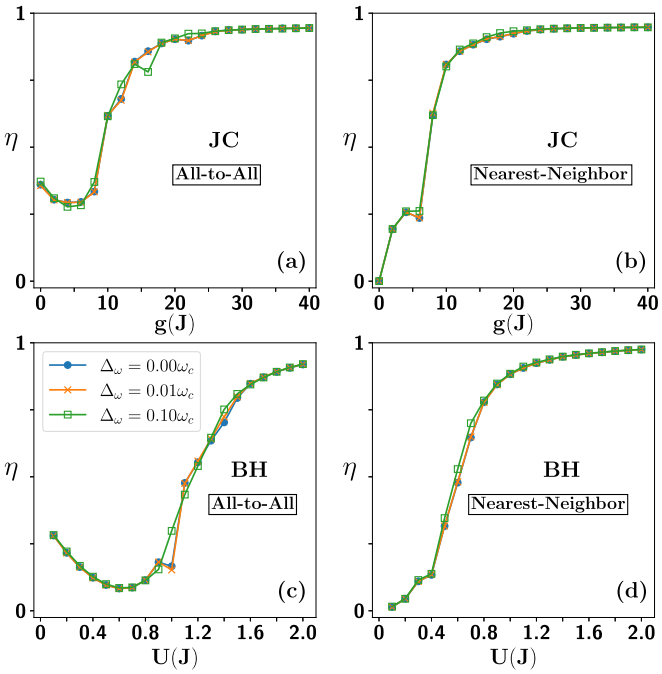

FIG. 10. Effect of disorder characterized by Δ_ω on the degree of localization for the exact quantum numerical solution. Results for $\Delta_\omega = 0.00$, 0.01, and $0.10\omega_c$ are compared. (a) and (b) show η as a function of g (in units of J) for the JC network with $N = 5$ and $N_p = 10$, for all-to-all and nearest-neighbor coupling, respectively. (c) and (d) show η as a function of U (in units of J) for the BH network with $N = 5$ and $N_p = 10$, for all-to-all and nearest-neighbor coupling, respectively.

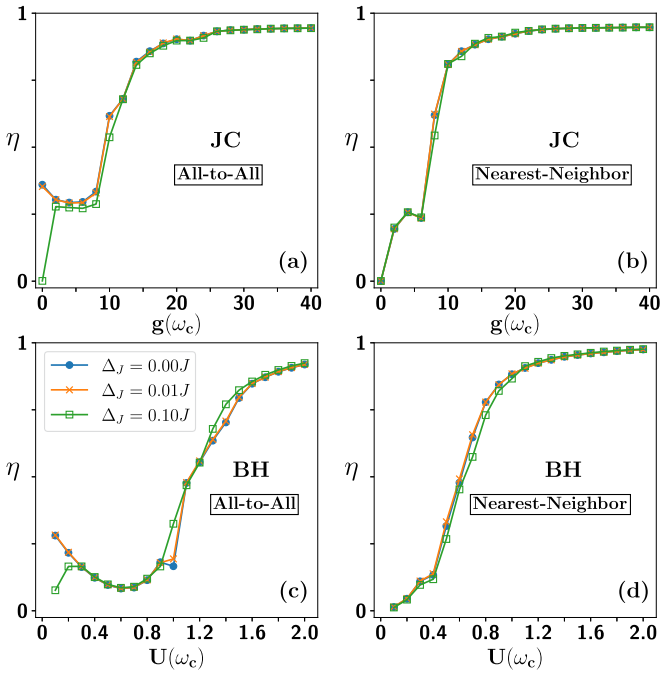

FIG. 11. Effect of disorder of the kinetic hopping J characterized by Δ_J on the degree of localization for the exact quantum numerical solution. Results for $\Delta_J = 0.00$, 0.01, and $0.10J$ are compared. (a) and (b) show η as a function of g (in units of ω_c) for the JC network with $N = 5$ and $N_p = 10$, for all-to-all and nearest-neighbor coupling, respectively. (c) and (d) show η as a function of U (in units of ω_c) for the BH network with $N = 5$ and $N_p = 10$, for all-to-all and nearest-neighbor coupling, respectively.

be obtained by putting $\gamma = \gamma_\phi = 0$ in Eq. (C1). Since, in the open-system case, the total number of excitations is not conserved, we introduce a slightly modified variant of $P(t)$, which is

$$Z(t) = \frac{P(t)}{\sum_{j=0}^{N-1} n_j(t)}. \tag{C2}$$

$Z(t)$ gives the ratio of the imbalance to the total number of excitations at any given time. In Fig. 9, this is plotted both for the JC network [Figs. 9(a) and 9(b)] and for the BH network [Figs. 9(c) and 9(d)]. We notice that self-trapping in both cases [Figs. 9(b) and 9(d)] persists for reasonably long times, after which there is a decay of $Z(t)$.

APPENDIX D: ROBUSTNESS TO DISORDER

The role of disorder due to error margins in parameter values of the network is discussed in this Appendix. In experiments, it is almost impossible to design network elements such as cavities and qubits of a given frequency or level gap without any error margin. For example, in a typical experiment, to design a cavity of frequency $\omega_c = 7 \times 2\pi$ GHz, there is an error margin of $\pm 70 \times 2\pi$ MHz ($0.01\omega_c$). Throughout this paper we have neglected such disorders in the network, and one might wonder about the consequence of disorder on the phenomenon of self-trapping. Thus, for our theoretical findings to be observed in potential experimental setups, it is important to check their robustness upon the inclusion of disorder. In order to proceed, we modify the cavity Hamiltonian in the following manner:

$$H_{\text{cavity}}^{\text{disord.}} = \sum_{i=0}^{N-1} (\omega_{c_i} + \epsilon_i) a_i^\dagger a_i, \tag{D1}$$

where ϵ_i is drawn from a uniform distribution ranging from $-\Delta_\omega$ to Δ_ω. In Fig. 10, we plot the degree of localization η as a function of the light-matter interaction g for the JC network and the on-site attractive potential U for the BH network. We present exact quantum numerical results for all-to-all and nearest-neighbor connectivity with $\Delta_\omega = 0.01$ and $0.1\omega_c$. The effect of disorder on the kinetic hopping strength J is also investigated by considering the hopping between two units i and j to be $J_{ij} = J + \epsilon_{ij}$, where $\epsilon_{ij} = \epsilon_{ji}$ is again drawn from a uniform distribution ranging from $-\Delta_J$ to Δ_J. In Fig. 11 we present the degree of localization for the JC and BH networks with all-to-all and nearest-neighbor coupling with $\Delta_J = 0.01$ and $0.1J$. The robustness to disorder in both cavity frequency and kinetic hopping is clearly manifested in Figs. 10 and 11.

[1] G. J. Milburn, J. Corney, E. M. Wright, and D. Walls, Phys. Rev. A **55**, 4318 (1997).

[2] S. Raghavan, A. Smerzi, S. Fantoni, and S. R. Shenoy, Phys. Rev. A **59**, 620 (1999).

[3] A. Smerzi, S. Fantoni, S. Giovanazzi, and S. R. Shenoy, Phys. Rev. Lett. **79**, 4950 (1997).

[4] S. Levy, E. Lahoud, I. Shomroni, and J. Steinhauer, Nature (London) **449**, 579 (2007).

[5] M. Albiez, R. Gati, J. Fölling, S. Hunsmann, M. Cristiani, and M. K. Oberthaler, Phys. Rev. Lett. **95**, 010402 (2005).

[6] K. Xhani, L. Galantucci, C. Barenghi, G. Roati, A. Trombettoni, and N. Proukakis, New J. Phys. **22**, 123006 (2020).

[7] D. O'Dell, Phys. Rev. Lett. **109**, 150406 (2012).

[8] I. A. Shelykh, D. D. Solnyshkov, G. Pavlovic, and G. Malpuech, Phys. Rev. B **78**, 041302(R) (2008).

[9] M. I. Makin, J. H. Cole, C. D. Hill, A. D. Greentree, and L. C. L. Hollenberg, Phys. Rev. A **80**, 043842 (2009).

[10] M. Abbarchi, A. Amo, V. Sala, D. D. Solnyshkov, H. Flayac, L. Ferrier, I. Sagnes, E. Galopin, A. Lemaître, G. Malpuech, and J. Bloch, Nat. Phys. **9**, 275 (2013).

[11] R. Coto, M. Orszag, and V. Eremeev, Phys. Rev. A **91**, 043841 (2015).

[12] S. Schmidt, D. Gerace, A. Houck, G. Blatter, and H. E. Türeci, Phys. Rev. B **82**, 100507(R) (2010).

[13] J. Raftery, D. Sadri, S. Schmidt, H. E. Türeci, and A. A. Houck, Phys. Rev. X **4**, 031043 (2014).

[14] A. Dey and M. Kulkarni, Phys. Rev. A **101**, 043801 (2020).

[15] K. Wright, K. M. Beck, S. Debnath, J. Amini, Y. Nam, N. Grzesiak, J.-S. Chen, N. Pisenti, M. Chmielewski, C. Collins, K. M. Hudek, J. Mizrahi, J. D. Wong-Campos, S. Allen, J. Apisdorf, P. Solomon, M. Williams, A. M. Ducore, A. Blinov, S. M. Kreikemeier *et al.*, Nat. Commun. **10**, 5464 (2019).

[16] C. Song, K. Xu, H. Li, Y.-R. Zhang, X. Zhang, W. Liu, Q. Guo, Z. Wang, W. Ren, J. Hao, H. Feng, H. Fan, D. Zheng, D.-W. Wang, H. Wang, and S.-Y. Zhu, Science **365**, 574 (2019).

[17] K. Xu, Z.-H. Sun, W. Liu, Y.-R. Zhang, H. Li, H. Dong, W. Ren, P. Zhang, F. Nori, D. Zheng, H. Fan, and H. Wang, Sci. Adv. **6**, eaba4935 (2020).

[18] S. Hazra, A. Bhattacharjee, M. Chand, K. V. Salunkhe, S. Gopalakrishnan, M. P. Patankar, and R. Vijay, Phys. Rev. Appl. **16**, 024018 (2021).

[19] K. Xu, Y.-R. Zhang, Z.-H. Sun, H. Li, P. Song, Z. Xiang, K. Huang, H. Li, Y.-H. Shi, C.-T. Chen, X. Song, D. Zheng, F. Nori, H. Wang, and H. Fan, Phys. Rev. Lett. **128**, 150501 (2022).

[20] Y. Lu, S. Zhang, K. Zhang, W. Chen, Y. Shen, J. Zhang, J.-N. Zhang, and K. Kim, Nature (London) **572**, 363 (2019).

[21] C. Figgatt, A. Ostrander, N. M. Linke, K. A. Landsman, D. Zhu, D. Maslov, and C. Monroe, Nature (London) **572**, 368 (2019).

[22] S. Debnath, N. M. Linke, C. Figgatt, K. A. Landsman, K. Wright, and C. Monroe, Nature (London) **536**, 63 (2016).

[23] C. Senko, J. Smith, P. Richerme, A. Lee, W. Campbell, and C. Monroe, Science **345**, 430 (2014).

[24] P.-C. Xu, J. W. Rao, Y. S. Gui, X. Jin, and C.-M. Hu, Phys. Rev. B **100**, 094415 (2019).

[25] F. Borjans, X. Croot, X. Mi, M. Gullans, and J. Petta, Nature (London) **577**, 195 (2020).

[26] S. Ritter, C. Nölleke, C. Hahn, A. Reiserer, A. Neuzner, M. Uphoff, M. Mücke, E. Figueroa, J. Bochmann, and G. Rempe, Nature (London) **484**, 195 (2012).

[27] V. D. Vaidya, Y. Guo, R. M. Kroeze, K. E. Ballantine, A. J. Kollár, J. Keeling, and B. L. Lev, Phys. Rev. X **8**, 011002 (2018).

[28] V. Giovannetti, D. Vitali, P. Tombesi, and A. Ekert, Phys. Rev. A **62**, 032306 (2000).

[29] M. Fitzpatrick, N. M. Sundaresan, A. C. Y. Li, J. Koch, and A. A. Houck, Phys. Rev. X **7**, 011016 (2017).

[30] F. Arute, K. Arya, R. Babbush, D. Bacon, J. C. Bardin, R. Barends, R. Biswas, S. Boixo, F. G. Brandao, D. A. Buell, B. Burkett, Y. Chen, Z. Chen, B. Chiaro, R. Collins, W. Courtney, A. Dunsworth, E. Farhi, B. Foxen, A. Fowler *et al.*, Nature (London) **574**, 505 (2019).

[31] H. J. Kimble, Nature (London) **453**, 1023 (2008).

[32] A. Dey, M. Q. Lone, and S. Yarlagadda, Phys. Rev. B **92**, 094302 (2015).

[33] Y. Li and S. C. Benjamin, npj Quantum Inf. **4**, 25 (2018).

[34] A. W. Chin, A. Datta, F. Caruso, S. F. Huelga, and M. B. Plenio, New J. Phys. **12**, 065002 (2010).

[35] Y.-C. Cheng and G. R. Fleming, Annu. Rev. Phys. Chem. **60**, 241 (2009).

[36] P. Wang, Y. Zheng, X. Chen, C. Huang, Y. V. Kartashov, L. Torner, V. V. Konotop, and F. Ye, Nature (London) **577**, 42 (2020).

[37] Y. Cao, V. Fatemi, A. Demir, S. Fang, S. L. Tomarken, J. Y. Luo, J. D. Sanchez-Yamagishi, K. Watanabe, T. Taniguchi, E. Kaxiras, R. C. Ashoori, and P. Jarillo-Herrero, Nature (London) **556**, 80 (2018).

[38] Y. He, R. Mao, H. Cai, J.-X. Zhang, Y. Li, L. Yuan, S.-Y. Zhu, and D.-W. Wang, Phys. Rev. Lett. **126**, 103601 (2021).

[39] M. Boissonneault, J. M. Gambetta, and A. Blais, Phys. Rev. A **79**, 013819 (2009).

[40] T. Zibold, E. Nicklas, C. Gross, and M. K. Oberthaler, Phys. Rev. Lett. **105**, 204101 (2010).

[41] A. Dey and A. Vardi, Phys. Rev. A **95**, 033630 (2017).

[42] M. Chuchem, K. Smith-Mannschott, M. Hiller, T. Kottos, A. Vardi, and D. Cohen, Phys. Rev. A **82**, 053617 (2010).

[43] P. W. Anderson, Phys. Rev. **109**, 1492 (1958).

[44] N. F. Mott, Rev. Mod. Phys. **40**, 677 (1968).

[45] R. Abou-Chacra, D. Thouless, and P. Anderson, J. Phys. C: Solid State Phys. **6**, 1734 (1973).

[46] G. Biroli, G. Semerjian, and M. Tarzia, Prog. Theor. Phys. Suppl. **184**, 187 (2010).

[47] V. Kravtsov, B. Altshuler, and L. Ioffe, Ann. Phys. (Amsterdam) **389**, 148 (2018).

[48] K. Tikhonov and A. Mirlin, Ann. Phys. (Amsterdam) **435**, 168525 (2021).

[49] K. Klocke, C. D. White, and M. Buchhold, Phys. Rev. B **104**, 214205 (2021).

[50] P. Prelovšek, M. Mierzejewski, J. Krsnik, and O. S. Barišić, Phys. Rev. B **103**, 045139 (2021).

[51] G. De Tomasi, F. Pollmann, and M. Heyl, Phys. Rev. B **99**, 241114(R) (2019).

[52] P. Prelovšek, O. S. Barišić, and M. Mierzejewski, Phys. Rev. B **97**, 035104 (2018).

[53] A. W. Cross, L. S. Bishop, S. Sheldon, P. D. Nation, and J. M. Gambetta, Phys. Rev. A **100**, 032328 (2019).

[54] T. Onodera, E. Ng, and P. L. McMahon, npj Quantum Inf. **6**, 48 (2020)..

[55] R. Nandkishore and D. A. Huse, Annu. Rev. Condens. Matter Phys. **6**, 15 (2015).

[56] J. Smith, A. Lee, P. Richerme, B. Neyenhuis, P. W. Hess, P. Hauke, M. Heyl, D. A. Huse, and C. Monroe, Nat. Phys. **12**, 907 (2016).
[57] A. Dey and M. Kulkarni, Phys. Rev. Res. **2**, 042004(R) (2020).
[58] M. Prasad, H. K. Yadalam, C. Aron, and M. Kulkarni, Phys. Rev. A **105**, L050201 (2022).
[59] A. J. Kollár, M. Fitzpatrick, and A. A. Houck, Nature (London) **571**, 45 (2019).
[60] A. J. Kollár, M. Fitzpatrick, P. Sarnak, and A. A. Houck, Commun. Math. Phys. **376**, 1909 (2020).
[61] J. Koch, M. Y. Terri, J. Gambetta, A. A. Houck, D. I. Schuster, J. Majer, A. Blais, M. H. Devoret, S. M. Girvin, and R. J. Schoelkopf, Phys. Rev. A **76**, 042319 (2007).
[62] A. A. Houck, H. E. Türeci, and J. Koch, Nat. Phys. **8**, 292 (2012).
[63] R. K. Naik, N. Leung, S. Chakram, P. Groszkowski, Y. Lu, N. Earnest, D. C. McKay, J. Koch, and D. I. Schuster, Nat. Commun. **8**, 1904 (2017); **9**, 172(E) (2018).
[64] A. Purkayastha, A. Dhar, and M. Kulkarni, Phys. Rev. A **93**, 062114 (2016).